ADVANCED VERY HIGH RESOLUTION RADIOMETER (AVHRR) DATA EVALUATION FOR USE IN MONITORING VEGETATION, VOLUME I - CHANNELS 1 AND 2

N. C. Horvath
Lockheed Engineering and Management Services Co., Inc.
1830 NASA Road 1
Houston, Texas 77258

T. I. Gray and D. G. McCrary
National Oceanic and Atmospheric Administration
Early Warning/Crop Condition Assessment Project Office
USDA, 1050 Bay Area Blvd.
Houston, Texas 77058

ABSTRACT

Data from the National Oceanic and Atmospheric Administration satellite system (NOAA-6 satellite) have been analyzed to study their nonmeteorological uses. The useful limits of these data were also determined. A file of charts, graphs, and tables was created from the products generated in this study. It was found that the most useful data lie between pixel numbers 400 and 2000 on a given scan line. The analysis of the generated products indicates that the Gray-McCrary Index can discern vegetation and associated daily and season changes. The solar zenith-angle correction used in previous studies was found to be a useful adjustment to the index. The Metsat system seems best suited for providing large-area analyses of surface features on a daily basis.

INTRODUCTION

The advanced very high resolution radiometer (AVHRR) system aboard the NOAA-6 satellite can simultaneously observe reflective energy in selected bandwidths of the visible and near-infrared parts of the solar spectrum (similarly to the Landsat MSS system) and can provide data relevant to agriculture. These new uses of the Metsat would complement the higher resolution Landsat data and provide more timely coverage.

Currently, the Foreign Crop Condition Assessment Division (FCCAD) of the U.S. Department of Agriculture, Foreign Agriculture Service (USDA/FAS) processes an index similar to the GMI in real time; however, the restraints and limits applicable to such indexes are unknown. The primary purpose of this study is to define these limits of acceptability for Metsat data.

POLAR ORBITING ENVIRONMENTAL SATELLITE CHARACTERISTICS

The data used in this study were collected by the NOAA-6 satellite and recorded at Wallops Island, Virginia, from

real-time transmission. These data are identical in content to the Local Area Coverage (LAC) data. The major differences between the Landsat MSS and the NOAA AVHRR systems are an image resolution at nadir, image width, and temporal continuity.

The AVHRR spectral bandwidths of the reflective channels, 1 and 2, were chosen to aid in the detection of snowmelt, an environmental phenomenon relative to hydrological forecasting. Channel 1 responds to reflected energy in the yellow-red portion (550-700 nm) of the visible spectrum and thus has a minimum response to verdant greens. However, the channel 2 bandwidth responds to the reflected energy in the near-infrared part of the spectrum (700-1100 nm) and acquires high values from vegetation.

THE GRAY-MCCRARY INDEX

The GMI is defined as the difference in the returns from channels 2 and 1. This index, which emphasizes the variations of healthy vegetation and provides negative responses for clouds and water, is relatively simple and can easily be placed into current operational activities.

Both clouds and water generate higher returns in channel 1 than in channel 2, consequently producing negative GMI values. For both channels, the cloud returns are high and the water returns are low, thus permitting the implementation of an analytical tool, "ramps." These ramps substitute one value for a variable negative result based upon the characteristics of channel 1.

We chose to set all cloud values (channel 1 response of 9% or greater) to a ramp of -1.5; all water, snow, and ice values to a ramp of -0.5; and certain indeterminate targets to -1.0. This approach reduces the emphasis of these targets and accentuates the remaining positive quantities for vegetation.

The GMI value was calculated for each pixel over the study area. A solar zenith angle correction was applied to the GMI values to simulate a condition of the same sun angle, regardless of the actual sun angle. The equation for the corrected GMI value is:

$$GMI^* = GMI(\sec^2 z)(\cos 39^\circ)(10)$$

where GMI* is the corrected GMI values and z is the solar zenith angle for the given pixel location. The value of 39° was chosen to adjust the data to the nominal solar zenith angle of Landsat scenes. The entire quantity was multiplied by 10 to facilitate data handling.

Generally, the values of the GMI vary from -1.5 to 32.0. Healthy vegetation produces values that range from about 8.0 upward. Soils have responses that vary from slightly less than zero to about 4.0 (ref. 5).

The most accurate values of the GMI occur for pure-pixel views. A mixed pixel will contain inputs from many

different sources, and thus the GMI value for that pixel will be altered. Pixels over pure vegetation give the highest return. A comparison of two pixels, one pure and one mixed, shows that the resultant GMI for the mixed pixel is less than that for the pure pixel.

THE TARGET AREA

Charts showing the 1979 distribution of major crops in Illinois are given in figure 1 (ref. 7). While these charts are not for 1980, previous charts reveal that the specific growing regions have changed very little.

A grid system shown in fig. 2, was placed over a map of this region to subdivide the acquisition into smaller sections and provide a basis for analysis. The i,j-grid system is a superset of the grid devised by Charney in 1952 (ref. 8) for computer analyses of meteorological data. This superset has the same orientation of that grid system where the i lines are parallel to 80° W. and the j lines to 170° W.

ANALYSIS AND INTERPRETATION OF RESULTS

In a study of this type, all available relevant data should be examined. The use of multiple methods of analysis is far more advantageous than dependence upon one particular system or procedure.

Scatterplots

A total of 33 scatterplots, plotting channel 2 versus channel 1, was produced to determine the AVHRR responses to various surface conditions. This effort includes a look at temporal changes in the GMI values and the results are presented in Table 1. The July ranges are all greater than those of October. In July, the natural vegetation and crops (corn and soybeans) appear green and thus have GMI values in the 6 to 10 range. The October ranges (2 to 3) seem to depict harvested fields (bare soil) and the autumn coloring of the forest. The areas surveyed in October might include bare trees, thus making the ground visible to the sensor.

The wide range of GMI values for the St. Louis area seems to indicate that the city includes large areas of trees and parkland. Thes tree-covered areas would explain the resemblance of some city plots to those of forest and cropland and would account for the change in GMI range for data gathered in autumn.

Nine of the scatterplots show some degree of cloud contamination. Most of these plots are from July periods, when there was some frontal activity in Illinois. While it is easy to guage the effect of large cloud fields, it is difficult to assess the contamination due to subresolution

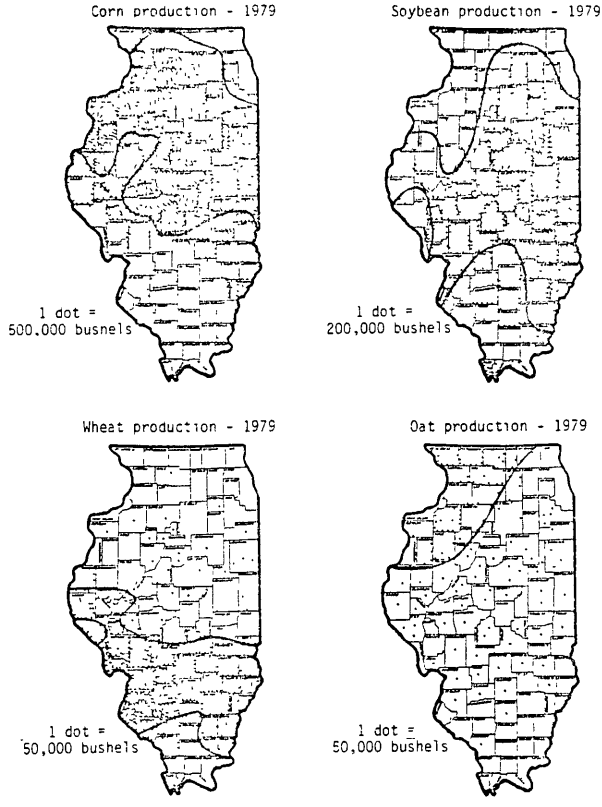

Figure 1. - Distribution of Major Crops (Ref. 7).

cloudiness. These clouds will contaminate otherwise high-value pixels, producing mixed pixels with lower returns, altering the surface appearance.

GMI* Data Analysis

The charts of the GMI* values were produced to examine spatial and temporal changes in the index over the target area. One chart was made for each day in both the July and October periods.

A persistent minimum feature was found in the data collected for St. Louis during the July period. This seems to be reasonable, because a city consists of concrete, asphalt, and other surfaces that offer lower returns than does vegetation.

Temporal changes in the GMI* were observed after rainfall. During the 24-hour peirod after the rain fell on July 10, the GMI* values were low for the specific area covered by precipitation (northwest section of the target area). In the following 24 hours an increase in the GMI* values was

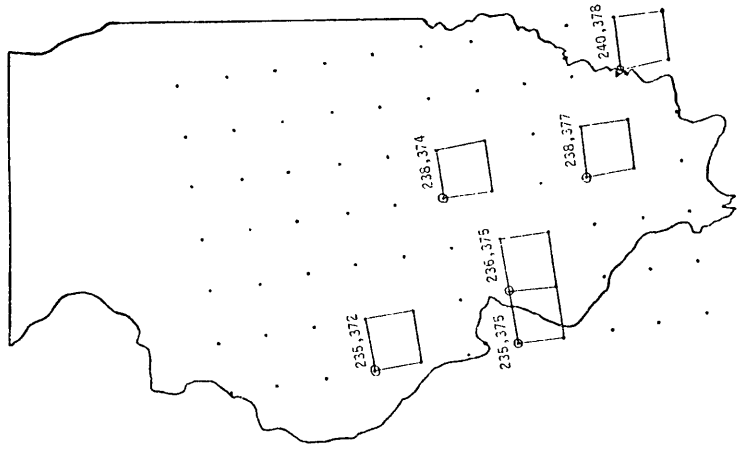

Figure 2. - Grid Cells (i,j) Used for Scatterplots.

observed for the same area. This change can be explained by considering surface conditions during this time period: For the 24-hour period immediately after the rain fell, the ground and plants probably were still wet, thus producing low-return signatures and subsequent low GMI* values. Then, in the next 24 hours, when surface conditions had become drier, the plants appeared greener, either having benefitted from the additional moisture, or having become cleaner because the rain washed any dust and dirt off the plants.

Solar Zenith-Angle and Pixel Considerations

It has been found that views with low pixel numbers (below 400) tend to have excessively high GMI* values. This is due to the solar zenith-angle correction, sec z, which increases rapidly above 70°. Illumination of the target does not change above 70° according to the sec z correction.

Transection Analyses

Transections were made of both the corrected and uncorrected GMI values. While they have almost identical characteristics, the corrected GMI curve has a sharper slope than does the uncorrected GMI curve. The west-to-east slope of these curves (low pixel numbers to the west) might be explained by land forms and vegetative cover. Another factor to consider is the solar elevation angle when these data were collected. At 0700 the eastern half of the scan will be sensing forward-scattered radiation, and the western half of the scan will be sensing backscattered radiation.

TABLE 3-1.- RANGES OF GMI VALUES FOR GIVEN GRID SQUARES

Day	GMI value range					
	Good cropland and Illinois River i,j=235,372	Good cropland i,j=238,374	City of St. Louis i,j=236,375	Forest and Rend Lake i,j=238,377	Ohio and Wabash Rivers and forest i,j=240,378	City of St. Louis i,j=235,375
191	†5 to 7	†7 to 8				
192	†6 to 8	All cloud				
193	†8 to 10	7 to 9				
194	9	8 to 9				
195	†-3 to 7	†6 to 7				
195	†1 to 3, 7 to 9	†6 to 9			All cloud	
196	8 to 10	7 to 8				
197	8 to 10	8 to 9	8 to 9	7 to 9	8 to 9	5 to 9
280	2 to 3	2 to 3				
282	2 to 4	2 to 3				
283	2 to 3	2 to 3		2 to 3	2 to 3	
284	1 to 2	†0 to 2	2			

†Includes contamination by clouds.

Table 1. - RANGES OF GMI VALUES FOR GIVEN GRID SQUARES

Additionally, transections were made of the actual raw-pixel values from channels 1 and 2. All of these raw-pixel-value curves slope upward at the ends, while the central portions are rather flat. The end effects are the result of the Sun-Earth-satellite geometry. Thus, while pixel size does increase away from nadir, the predominant end effects are due to preferential scattering of the incident radiation. Because of this systematic end distortion, the flat, central part of each curve probably offers the most reliable data.

Resolution Deterioration Considerations

Graphs were drawn to display pixel deterioration away from nadir and to determine the usable portion of the scan line. Figure 3 shows that the largest range of values appears on the low-pixel-number end of the scan line. The collection of data begins in the west, or away from the Sun, and the data are collected toward the Sun. Because of the early morning acquisition time, the western end of the scan line is contaminated by shadows and the eastern part of the scan line is contaminated by sun glint. Also included here is a portion of the scan line covered by the Illinois target area. The location of the Illinois area on the scan line will determine the number of pixels included in said area. This difference is attributed to the way in which pixels change in size away from nadir, as shown in figure 4. At the edge of a scan line, the pixels are longer, thus covering more area individually.

These two graphs, in conjunction with the daily GMI* charts, were used to determine what parts of the scan line should be eliminated. If the central 1200 pixels are used and the outer portions are discarded (400 pixels on either end), the data remaining will be of good quality, thus eliminating extreme GMI* values and minimizing errors which are due to pixel size.

Data and Index Corrections

Calculations of the GMI values were performed both with and without a secant solar zenith-angle correction. In all cases the shapes of contours and patterns of lines were very similar. Even so, the correction will give all the data the same sun angle and make the comparisons, especially the monthly ones, much more valid.

The problem of atmospheric scattering and absorption was not considered in this study.

Charts of Weekly GMI* Maximums

Probably the best way to utilize this index is through the use of the analyzed fields of weekly GMI* maximums. GMI* maximums were selected to minimize atmospheric attenuation because high values of this index will coincide with relatively clear days. Figure 5 shows the GMI* maximums for the July and October acquisitions. In these particular charts, data from days which appeared on the low-pixel-number end of the scan were eliminated.

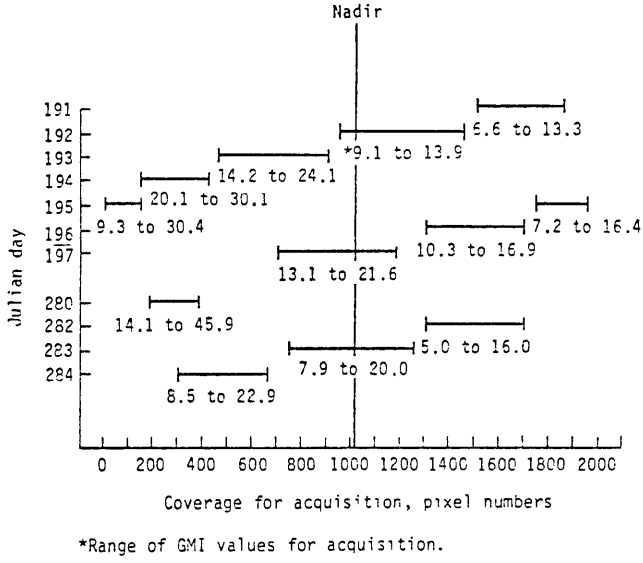

Figure 3. - Width and relation to nadir of each acquisition on a scan line

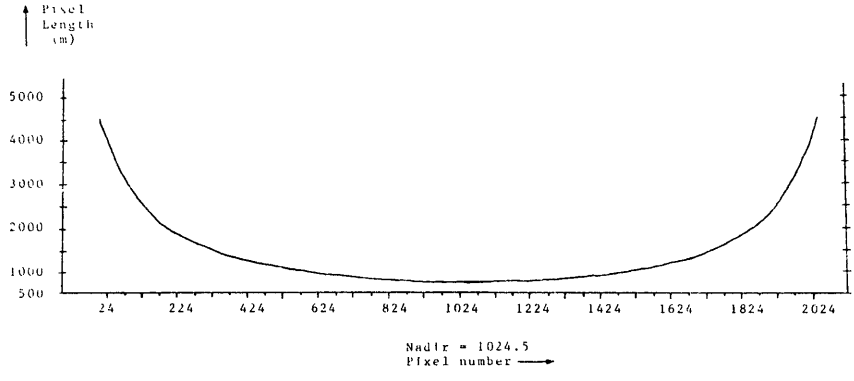

Figure 4. Plot of pixel length away from nadir (ref. 12).

The resulting patterns on these GMI value charts were then compared with the chart of the distribution of major crops (fig. 1) and with the agricultural analysis.

In July the central maximum area on the chart of GMI* values corresponds with the areas normally planted in corn and soybeans. The southern minimum areas correspond to the wheat-growing regions. The axis of the minimum area in the northwestern part of Illinois lies along the valley of the Illinois River, and a minimum value also appears for an area centered in St. Louis.

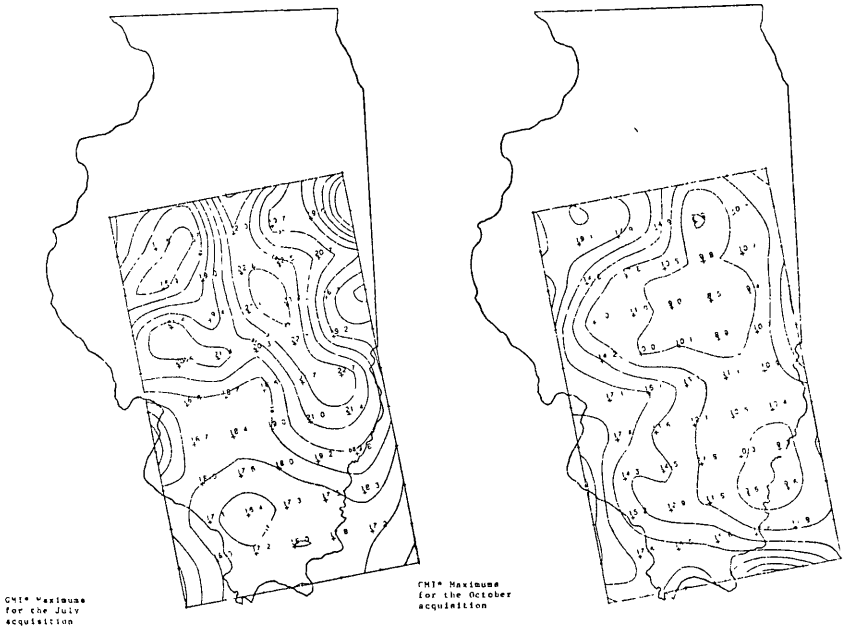

Figure 5. - Maximum GMI values

When the agricultural data analysis was examined, both the corn and soybeans were found to be reasonably healthy (high GMI* values); the wheat was almost completely harvested (low GMI* values); and the oats were turning yellow (low GMI* values).

For October, the central minimum area corresponds with the corn and soybean area, which at this time was more than 50 percent harvested (low GMI* values). The wheat areas were undergoing planting or plowing and consequently had a similar response (low GMI* values) to that for July. Since wheat is grown on a small scale in Illinois the low GMI* values over the wheat growing region might not reflect the health of that specific crop. However, this area did have some of the highest temperatures and the least amount of rainfall during the July and October acquisitions. Consequently, the low GMI* values there could indicate the amount of stress on all the vegetation.

These comparisons indicate that cultivated vegetation can be observed with the NOAA AVHRR. While the GMI produces broad-area estimtes and can make only a gross estimate of vegetative conditions, it oculd be a useful tool and adjunct to current operational systems.

REFERENCES

1. Gray, T. I., Jr. and D. G. McCrary, 1981, Meteorological Satellite Data - A Tool to Describe the Health of the World's Agriculture. AgRISTARS Report EW-N1-04042, JSC-17112, 7 pp.

2. Helfert, M. R., D. G. McCrary and T. I. Gray, 1981, Utilization of Meteorological Satellite Imagery for World-Wide Environmental Monitoring of the Lower Mississippi River Flood of 1979 - Case 1. AgRISTARS Report EW-N1-04104, JSC-17144, 26 pp.

3. McCrary, D. G, T. I. Gray and T. E. Armstrong, 1981, Characteristics of TIROS, GOES, DMSP and LANDSAT Systems, AgRISTARS Report EW-N1-04075, JSC-17131, LEMSCO-16504, 17 pp.

4. Gray, T. I., Jr, and D. G. McCrary, 1981, The Environmental Vegetation Index, a Tool Potentially Useful for Arid Land Management. AgRISTARS Report EW-N1-04076, JSC-17132, 3.

5. Gray, T. I., Jr., and D. G. McCrary, An Application of Advanced Very High Resolution Radiometer Data to Monitor the World's Agricutlure. (in press).

6. Kuchler, A. W., 1975, Potential Natural Vegetation of the Conterminous United States, American Geographical Society, New York.

7. Illinois Agricutlural Statistics, Annual Summary, 1980. Illinois Cooperative Crop Reporting Service (Springfiled), 1980.

8. Charney, J. G. and N. A. Phillips, 1953, Numerical Integration of the Quasi-Geostrophic Equations for Barotropic and Simple Baroclinic Flaws, Journal of Meteorology, Vol 10, no. 2, pp. 71-99.

9. Thompson, D. R., and O. A. Wehmanen, 1979, Using Landsat Digital Data to Detect Moisture Stress. Photogrammetric Engineering and Remote Sensing, Vol. 45, No. 2, pp. 201-207.

10. Daily Weather Maps, Weekly Series. U.S. Dept. of Commerce, NOAA, Environ. Data and Information Service, July 7-13, 1980; July 14-20, 1980; Oct. 6-12, 1980.

11. Weekly Weather and Crop Bulletin. U.S. Department of Commerce, NOAA, Environmental Data and Information Service; USDA Economics, Statistics and Cooperative Service, Vol. 67, no. 29, July 15, 1980; vol. 67, no. 30, July 22, 1980; vol. 67, no. 42, Oct. 15, 1980.

12. Climatological Data. U.S. Dept. of Commerce, NOAA, Environmental Data and Information Service, National Climatic Center (Asheville, N.C.), Illinois vol. 85, no. 7; Indiana vol. 85, no. 7; Iowa vol. 91, no. 7; Kentucky vol. 75, no. 7; Missouri vol. 84, no. 7; July 1980; Illinois vol. 85, no. 10; Indiana vol. 85, no. 10; Kentucky vol. 75, no. 10; Oct. 1980.

13. Tappan, G., and G. E. Miller, 1982, Area Estimation of Environmental Phenomena from NOAA-n Satellite Data. AgRISTARS Report EW-L1-04190, JSC-17437, LEMSCO-17312, 41 pp.